Eur Biophys J (1996) 24: 125–135

European Biophysics Journal

Brownian dynamics simulation of the lateral distribution of charged membrane components

Dirk Walther[1,2], **Peter Kuzmin**[1,3], **Edwin Donath**[1]

[1] Institute of Biophysics, Department of Biology, Humboldt-University, Invalidenstrasse 42, D-10115 Berlin, Germany
[2] European Molecular Biology Laboratory, Meyerhofstrasse 1, D-69012 Heidelberg, Germany
[3] A. N. Frumkin-Institute of Electrochemistry of the Russian Academy of Sciences, Moscow, Russia

Received: 28 June 1995 / Accepted in revised form: 20 November 1995

Abstract. Brownian dynamics simulations were performed to study the contribution of electric interactions between charged membrane components to their lateral distribution in a two-dimensional viscous liquid (bilayer lipid membrane). The electrostatic interaction potential was derived from an analytical solution of the linearized Poisson-Boltzmann equation for point charges in an electrolyte solution - membrane - electrolyte solution system. Equilibrium as well as dynamic quantities were investigated. The lateral organization of membrane particles, modelled by mobile cylinders in a homogeneous membrane separating two electrolyte solutions was described by spatial distribution functions, diffusion coefficients and cluster statistics. Disorder, local order and crystal-like arrangements were observed as a function of the particle charge, the closest possible distances between the charges and the particle density. The simulations revealed that the system is very sensitive to the position of the charges with respect to the electrolyte solution - membrane interface. Electrostatic interactions of charges placed directly on the membrane surface were almost negligible, whereas deeper charges demonstrated pronounced interaction. Biologically relevant parameters corresponded at most to local and transient ordering. It was found that lateral electric forces can give rise to a preferred formation of clusters with an even number of constituents provided that the closest possible charge-charge distances are small. It is concluded that lateral electrostatic interactions can account for local particle aggregations, but their impact on the global arrangement and movement of membrane components is limited.

Key words: Membrane - Brownian dynamics simulation - Electrostatics - Debye-Hückel theory - Diffusion - Lateral distribution

Introduction

In biological membranes lipids form a two-dimensional liquid phase in which membrane proteins are embedded or to which they are attached. It is generally accepted that the lateral distribution and dynamics of membrane proteins and lipids are important for their biological functions such as ligand-stimulated membrane receptor aggregation in transmembrane signalling (Hendrickson 1992). Similarly, intermolecular helix-helix interactions are believed to be responsible for membrane protein oligomerization (Lemmon and Engelman 1992). To understand these processes, it is important to have a clear and detailed understanding of the driving forces and the underlying physical and biological principles of particle-particle interactions in membranes.

To describe the lateral organization of particles in biological membranes, numerous approaches have been applied. Besides indirect, lipid-mediated interactions of proteins (Marcelia 1976; Sperotto and Mouritson 1991; Mouritsen and Bloom 1993), direct particle-particle interactions have been frequently discussed. The range of the underlying interaction potentials varied from the avoidance of particle overlap and its effect on the diffusion coefficient (Pink et al. 1986; Karyakin 1989; Saxton 1994) to arbitrary potential functions and even detailed Molecular Dynamics simulations of lipid membranes (Abney and Owicki 1985; Egberts et al. 1994).

Electric fields are crucial to many membrane processes (Nelson and McQuarrie 1975; Honig et al. 1986; McLaughlin 1989; Brown 1990; Cevc 1990). To assess the significance of electrostatic forces on the dynamic lateral structure in membranes, we have studied their influence using Brownian dynamics simulations of a simplified model system. In particular, the biologically relevant conditions under which long-range interactions are possible were explored.

The efficiency of electric interactions at the electrolyte solution - membrane - electrolyte solution interface is controlled by several parameters including pH, ionic strengths of the adjacent electrolyte solutions, pK_a of titrating sites of interacting molecules and the position of membrane particle charges with respect to the membrane-solution interface. Consequently, the variation in strength of lateral electric interactions may serve as a regulatory system for membrane related processes. It is also noteworthy that surface diffusion and aggregation of particles became increasingly important

Correspondence to: D. Walther (e-mail: walther@embl-heidelberg.de)

for controlling small-scale structures in submicron technological applications (Jensen et al. 1994).

Computer simulation is a powerful technique to study the independent contribution of electric forces between membrane particles and to follow the formation of ordered structures of such particles in lipid membranes over time. The Brownian dynamics of particles in three-dimensional systems have been addressed by several authors (Northrup et al. 1988; Davis et al. 1991; Zhou 1993; Kozack et al. 1995), but to the best of our knowledge, the consideration of charged membrane particles has not yet been comprehensively treated. Therefore, we carried out a Brownian dynamics simulation of a model system consisting of charged model particles embedded in a two-dimensional liquid (membrane) separating two electrolyte solutions. The electric interaction potential was derived from an analytical solution of the linearized Poisson-Boltzmann equation for point charges in such an electrolyte solution - membrane - electrolyte solution system. We believe that the investigated model reflects all the principal features of long-range charge-charge interactions in biological membranes and the different regimes of lateral electric interactions revealed should help in understanding the dynamic behaviour of membranes.

Material and methods

The model

The model used here assumes a sandwich-like three-layered system consisting of two electrolyte solutions separated by a membrane as shown in Fig. 1. The membrane is considered as a plane-parallel dielectric layer of thickness d and a low dielectric constant ε_m. The electrolyte solutions are characterized by their ionic strengths I, a corresponding Debye parameter κ and by their dielectric constant ε_s. The ionic strengths were identical for both electrolyte solutions. The coordinate system used is oriented with the z-axis normal to the membrane's surface, with its origin in the middle plane of the membrane. Membrane particles are represented by cylinders with a radius R and the same height as the membrane d with cylinder axes parallel to the z-axis and the same dielectric constant as the membrane. The membrane particles carry α elementary electric charges q of a given sign located at defined z-positions (the same for all particles in the system) along the cylinder rotation axis. The particles are distributed within the membrane with an average particle density σ and are mobile in the membrane plane (xy-plane) only. The motion of a membrane particle is determined by two processes: 1) stochastic thermal motion with a diffusion coefficient D^o for particles in infinite dilution, and 2) migration in the electric field resulting from the charges of other charged particles as well as from the surrounding ionic atmosphere. Hydrodynamic effects have not been taken into account. Recent studies related to these effects have been shown to reconcile discrepancies between theoretically and experimentally determined diffusion coefficients (Brussel el al. 1995).

Interaction potential

Several approximate expressions for the electric potential caused by discrete charges in the electrolyte solution/membrane/electrolyte solution system have been reported (Nelson and McQuarrie 1975; Edmonds, 1988; Schnitzer and Lambrakis 1991; Frausto et al. 1992; Martinez and Sancho 1993; Clarke 1993; Forsten et al. 1994). In our simulations, we used expressions obtained for the electric potential around point charges in a three layer system presented earlier (Arakelian et al. 1993). The Debye-Hückel approach was applied and linearized Poisson-Boltzmanns equations were solved. This was justified by the low ionic strengths of the electrolyte solutions (I=100 mM in most cases) and the low mobility of the charge carrying particles with a diffusion coefficient $D_{particle}$ of $10^{-8} - 10^{-9}\mathrm{cm}^2/\mathrm{s}$, compared to the mobility of the ions of the adjacent electrolyte solution D_{ion} of $\approx 10^{-5}\mathrm{cm}^2/\mathrm{s}$ (see section parameter values). Thus, the ion clouds around the membrane particle charges may be assumed to be in equilibrium. An outline of the derivation of the analytical expressions for the electric potential is given in the Appendix. To prevent particle overlap, the electric interaction was replaced by an elastic repulsion term. The interaction energy V between two particles was calculated as

$$V_{el}(\rho) = \alpha_i \alpha_j q \varphi(\rho_{ij} \quad if \quad \rho_{ij} \geq 2R \tag{1}$$

and

$$V(\rho) = \alpha_i \alpha_j q \varphi(2R) + \frac{(2R - \rho_{ij})^2}{4u\delta t} \quad if \quad \rho_{ij} < 2R \tag{2}$$

where ρ_{ij} is the distance between two particles in the xy-plane, φ is the electric potential of an elementary charge q at the distance ρ_{ij} (see Appendix), α_i and α_j are the respective signed charge numbers and u is the mobility of the particle. The mobility u is related to the diffusion coefficient by $D^o = uk_B\mathrm{T}$ where k_B is the Boltzmann constant and T is the absolute temperature. The soft repulsive force was sufficient to keep colliding particles apart from one another. The deterministic additive forces $\vec{\mathbf{F}}_d$ acting on the particle i were derived from numerical differentiation of the interaction potential with respect to ρ such that

$$\vec{\mathbf{F}}_{d,i} = -\nabla \sum_{j,i\neq j} V(\rho_{ij}, \alpha_i, \alpha_j, z_i, d, I_1, I_3, \varepsilon_m, \varepsilon_s, T) \tag{3}$$

Except the particle density, Eq. (3) summarizes all relevant system parameters determining the electric interactions between the particles.

Simulation algorithm

Our goal was to study the time evolution of the system in order to determine the dynamic structuring and the kinetic behaviour of the system. Molecular dynamics simulations with an atomic description of the system appeared very expensive and time consuming. In any case, since we were not interested in the detailed characterization of the random collisions of our model particles with the surrounding lipid molecules, they were considered as a heat bath only. Thus,

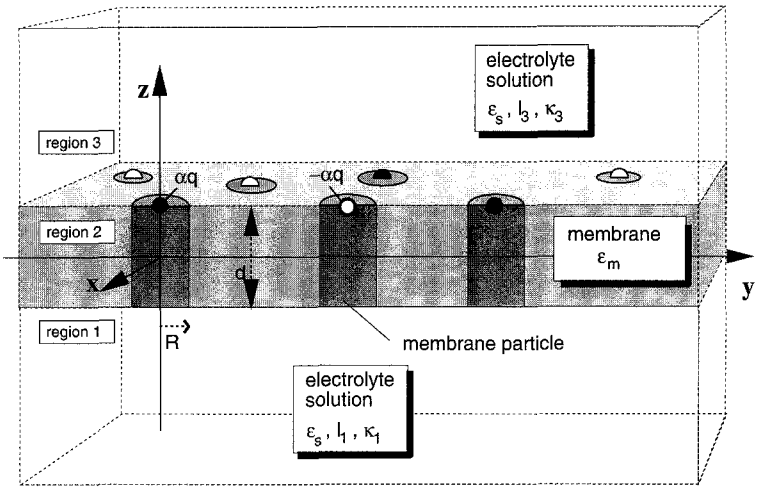

Fig. 1. Cross sectional view of the model system with the physical parameters of the model and the coordinate system used. The current location of the charges are depicted by the filled/open circles. The open circles represent charges of opposite sign as compared to the charges represented by the filled circles. The particles carry α elementary charges q. The properties of the electrolyte solutions are described by the dielectric constant ε_s, the ionic strengths I and, correspondingly, the Debye-Hückel parameter κ. The indices correspond to the respective regions in the system. The membrane is assigned a dielectric constant ε_m

the Brownian dynamics simulation technique omitting the solvent particles from the detailed simulation was appropriate to propagate our particle system through configurational space in time. Thus, Newton's equations of motion could be replaced by the Langevin equations as given in Eqs. (4) and (5):

$$\vec{\mathbf{v}} = \frac{d\vec{\rho}}{dt}, \tag{4}$$

$$m\frac{d\vec{\mathbf{v}}}{dt} - \beta\frac{d\vec{\rho}}{dt} = \vec{\mathbf{F}}_d(t) + \vec{\mathbf{F}}_s(t), \tag{5}$$

where $\vec{\mathbf{F}}_d$ is the deterministic electric force, $\vec{\mathbf{F}}_s$ is a stochastic force, β is the drag coefficient and m is the particle mass. Random collisions of the model particles with the surrounding lipids are represented by a combination of a stochastic force term $\vec{\mathbf{F}}_s(t)$ and a drag term. The drag coefficient β can be replaced by the reciprocal value of the mobility ($\beta = 1/u$) and in terms of the Einstein relation $\beta = (k_BT)/D^o$, where k_B is Boltzmann's constant and T is absolute temperature. The Brownian dynamics approach involves numerical integration of the system of Eqs. (4) and (5). If the inertial behaviour of the particles were of interest, the integration time step δt had to be much smaller than the autocorrelation time τ of the particle velocity. τ is given by

$$\tau = \int_0^\infty e^{-\frac{k_BT}{mD^o}}dt = \frac{mD^o}{k_BT}. \tag{6}$$

Assuming characteristic values for the parameters in Eq. (3), e.g. the transmembrane protein Band 3 of human erythrocytes with $D^o \approx 10^{-9}\mathrm{cm}^2/\mathrm{s}$, molecular weights of M=50-100 kDa and a temperature of 300 K, this correlation time corresponds to $\tau \approx 10^{-15}$s. Since we were interested in the simulation of the system over a longer time interval (10^{-3}s), the diffusion limit, Eq. (5) can be simplified by neglecting the drag term. One finally obtains the "Position Langevin Equation" introduced by Lax (1966) and Zwanzig (1969):

$$\frac{d\vec{\rho}}{dt} = \frac{D^o}{k_BT}\vec{\mathbf{F}}_d(t) + \frac{d\vec{\rho}_s}{dt}. \tag{7}$$

The term $d\rho_s/dt$ describes a random velocity process with a delta function as autocorrelation function (Allen and Tildesley 1987). Consequently, the time step δt guaranteeing a correct integration of the equation of motion could be increased up to 10^{-8}s. The Position Langevin Equation (Eq.(4)) was integrated by using the algorithm proposed by Ermak (1975). The position of a particle evolved as follows:

$$\vec{\rho}(t+\delta t) = \vec{\rho}(t) + \frac{D^o}{k_BT}\vec{\mathbf{F}}_d(t)\delta t + \delta\vec{\rho}_G, \tag{8}$$

where ρ is the position vector of a given particle in the xy-plane and $\delta\rho_G$ was obtained from a two dimensional Gaussian distribution with a mean equal to zero and the variance $< \delta\rho^2 >= 4D^o\delta t$. The values for the input diffusion coefficient D^o were taken from experimentally determined diffusion coefficients in a system of low particle density (see below in parameter values section). The time step δt was chosen such that maximal displacements of the particle in one dimension were small compared to the particles radius such that

$$\frac{D^o}{k_BT}F_d(2R)\delta t + 6\sqrt{2\delta t D^o} \leq 0.5R, \tag{9}$$

where $F_d(2R)$ is the electric force at particle-particle contact and δt is the maximal possible value satisfying the condition in Eq. (9). The simulation box represented a square patch of the membrane with box length L. Periodic boundary conditions were applied. A cutoff distance for interparticle interactions (ρ_{cutoff}) was selected such that the pairwise electrostatic energy decayed below the value of $k_BT/10$ at this distance. The cutoff distance was required to be minimally $8R$ and maximally $L/2$. Because of the large size of the simulation systems, the utilization of the upper boundary for cutoff was always avoided. To reduce the computation time, a neighbour list was introduced for every particle (Allen and Tildesley 1987) with a cutoff distance ρ_{cutoff}. The neighbour list was updated every tenth time step. Starting from a random particle distribution and after equilibration which required at most 500000 cycles for strongly interacting particles, the system was simulated over an acquisition time t_a. This time corresponds to time intervals in which non-interacting particles diffused on average a distance of $50R$ as

calculated from the Einstein-Smoluchowski relation for two-dimensional diffusion $t_a = (50R)^2/(4D^o)$; i.e. of the order of milliseconds given values of D^o as described below. Control runs starting from initially regular particle assemblies eventually resulted in qualitatively identical particle distributions. The results presented were obtained by averaging over three independent runs for each system examined.

Structural and kinetic quantities

In the field of statistico- mechanical physics, various correlation functions are used to describe the spatial order of fluid systems. We calculated the radial distribution function $g(\rho)$, the orientionally averaged part of the correlation function $g(\mathbf{r})$. To exclude trivial spatial effects caused by excluded volume, $g(\rho)$ was normalized to the radial distribution function of randomly distributed non-overlapping particles $g_{rnd}(\rho)$.

$$g(\rho) = \frac{\langle \sum_i \sum_{j \neq i} \delta(\rho - \rho_{ij}) \rangle}{g_{rnd}(\rho)}. \tag{10}$$

where δ is the Dirac's delta function. During the computations δ was replaced by a small radial increment $\Delta r = R/5$. $g_{rnd}(\rho)$ was obtained from simulations without electric interactions but with elastic repulsion (Eq. (2)) and is simply given by

$$g_{rnd}(\rho) = \langle \sum_i \sum_{j \neq i} \delta(\rho - \rho_{ij}) \rangle. \tag{11}$$

The commonly used expression $g_{rnd}(\rho) = N\pi\sigma((\rho+\Delta\rho)^2 - \rho^2)$ where σ is the particle density was not suitable because of the finite particle radius. Apart from quantitative aspects of depletion and accumulation of particles, $g(\rho)$ gives insight into the range of lateral order. Short range order will result in peaks near $\rho = 2R$ only, whereas long range order will be represented by multiple peaks. The radial distribution function $g(\rho)$ was calculated every 50th time step for systems in equilibrium, with subsequent averaging. Thus, correlations between consecutive configurations were reduced

The static and dynamic clustering of the system was quantified using the following cluster counting algorithm. A particle was considered to belong to a cluster if the distance of closest approach d_c to at least one neighbouring particle was less than 0.5 nm, within which protein-protein interactions are largely determined by short-range forces and chemical processes. Furthermore, the lipid matrix cannot be considered as a continuum below this range. The cluster frequency as a function of time and the cluster size distribution function (CSD), the mean frequency of clusters of a certain size, were also calculated. The former provides information about the rate of global lateral structural changes. Clusters may disappear either through dissociation into smaller units or association into larger clusters and hence their persistence was monitored at a characteristic interval of time Δt_{char}. This interval was adjusted such that freely moving, non-interacting particles diffuse on average over a distance of 1/10 of d_c in this period of time; i.e., $\Delta t_{char} = d_c^2/(40D^o)$. If necessary, the integration time step of simulation δt was adjusted to smaller values so that $5\delta t \leq \Delta t_{char}$ was always fulfilled. If a cluster was identified as unmodified, its life time was prolonged by Δt_{char} or otherwise, the cluster species counter was incremented by one and the lifetime of the new cluster was initialized by Δt_{char}. It was assumed that the particles in the system are distinguishable so that a cluster was not only defined by its size but also by its actual constituents. The cluster lifetime characterizes the local, electrostatically mediated stability of the system and indicates whether other processes such as chemical reactions or transport processes have sufficient time to proceed. The kinetic behaviour of the particle system was characterized by the diffusion coefficient D *via* the Einstein-Smoluchowski relation for two-dimensional diffusion, $D = \langle \rho^2 \rangle / 4\Delta t$. The mean square deviations from initial positions, $\langle \Delta\rho^2 \rangle$ were obtained by comparing starting and final positions of the particles without application of the periodic boundary condition.

Parameter values

The strength of lateral electric interactions of charged membrane particles is influenced by a number of factors such as the charge numbers, ionic strengths of the electrolyte solutions separated by the membrane, the sterically permitted closest distances between charges, the particle density, the location of the charges with respect to the membrane/solution interface, the dielectric constants and the temperature. In order to obtain biologically relevant results, the range of parameters were confined to biologically reasonable conditions. The thickness of the membrane was taken as 5 nm. The dielectric constant ε_m of the membrane was assumed as 3 and 80 for the electrolyte solution (ε_s). The temperature in both the electrostatic potential calculations and in the Brownian dynamics simulations was 310 K. Two different particle populations distinguished by their respective radii were investigated. One with a radius R of 0.5 nm corresponding to the approximate radius of a phospholipid molecule or a single membrane-spanning protein α-helix. Another particle type with R = 1.5 nm was taken to represent a membrane protein of small to medium size with a molecular weight of about 20–50 kDa. For these two particle systems, the respective input diffusion constants D^o were 10^{-8}cm^2/s for the smaller and 10^{-9}cm^2/s for the larger particles (Gennis 1989; Clegg and Vaz 1985). The density of the particles σ was kept within a biological range and was generally assumed as 0.02 nm^{-2}. All simulations were run with 500 particles in a simulation box of appropriate size calculated from the particle density and number of particles.

Results

Investigations commenced with control simulations without electric interactions at particle densities of 0.02 nm^{-2} and 0.04 nm^{-2}. These values correspond to a distance of approximately 7 nm for the former and 5 nm between the nearest neighbours on a square lattice. Assuming a particle radius of 1.5nm (0.5nm) the diffusion coefficient decreased to 78.2% (98.4%) of the input diffusion coefficient D^o. At

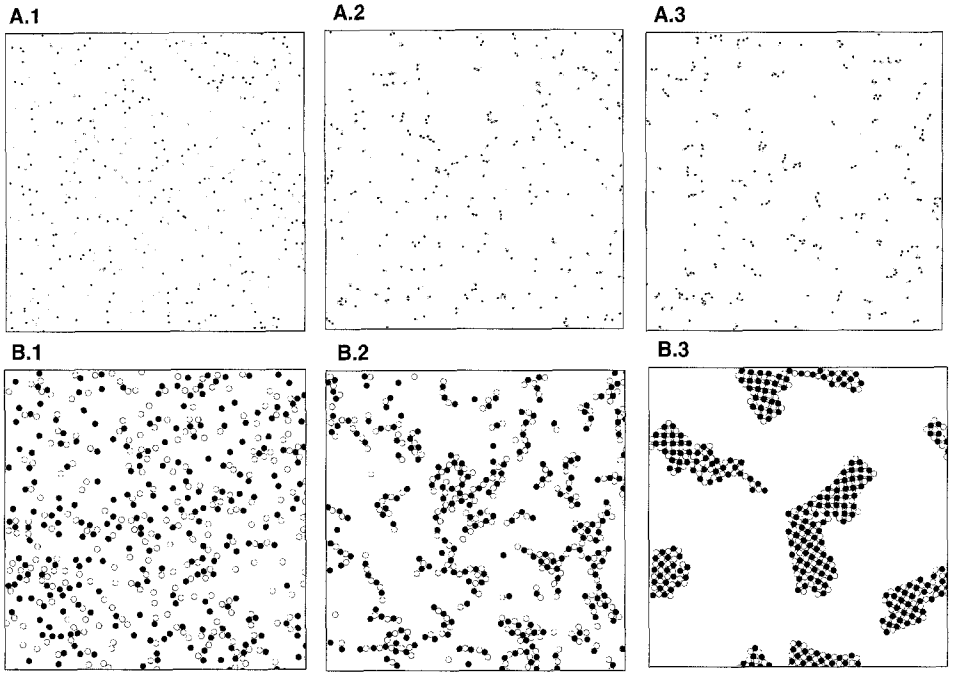

Fig. 2. Simulation snapshots of an oppositely charged particle system. **A** particle radius R=0.5 nm, A.1 - charge directly onto the membrane surface, A.2 - charge 1.0 nm beneath the surface, A.3 - charge in the middle plane of the membrane, I=100 mM, σ = 0.02 nm^{-2}, D^o = 10^{-8}cm^2/s; **B** charge position in the middle plane of the membrane, radius R=1.5 nm, σ = 0.02 nm^{-2}, I=100 mM, D^o = 10^{-9}cm^2/s, B.1, B.2, B.3 correspond to the charge numbers α = 1,2 and 3, respectively. The instantaneous mean potential energies per particle $\langle V_{sum}/N \rangle$ in units of k_BT were -0.04, -6.13 and -9.84 for snapshots A.1, A.2 and A.3 and for the snapshots B.1, B.2 and B.3 $\langle V_{sum}/N \rangle$= -0.8, -7.8 and -28.3, respectively

σ = 0.04 nm^{-2} it decreased to 60.5% (91.4%), respectively. Given these particle densities, lateral order is more likely to be caused by electrostatic particle attraction rather than repulsion. Assuming close contacts between oppositely charged particles, the characteristic interaction distance is smaller than the typical Debye length (1-10 nm) while in the case of repulsion for equally charged particles, the mean distance between the charges is large. The interaction energy would decay to small values as compared to k_BT at these distances of separation. Consequently, the simulations focused on particle systems consisting of an equal number of positively and negatively charged particles.

Static (equilibrium) properties

The snapshots shown in Fig. 2 give an impression of the qualitative behaviour of the simulated particle system. As a function of the increasing interaction by positioning the charges into the membrane or increasing the charge, the transition from a randomly distributed particle system to a well structured system, finally demonstrating two-dimensional crystallization, can be observed.

Figure 3 summarizes the radial distribution functions obtained for particle systems with a radius of 0.5nm. The lateral ordering was drastically increased when the charges were located inside the membrane region (Fig. 3A), particularly for middle membrane plane charges where a pronounced lateral correlation at the characteristic second neighbour distance and a weak third neighbour correlation was observed. This is in sharp contrast to positioning the charges directly onto the membrane's surface. Even by reducing the screening of the charge-charge interactions by lowering the ionic strength of the electrolyte solutions from 100 mM to 1 mM, the lateral correlations were almost negligible (Fig. 3B).

The dielectric constant of the membrane naturally affects the lateral organization of charged particles. The far reaching

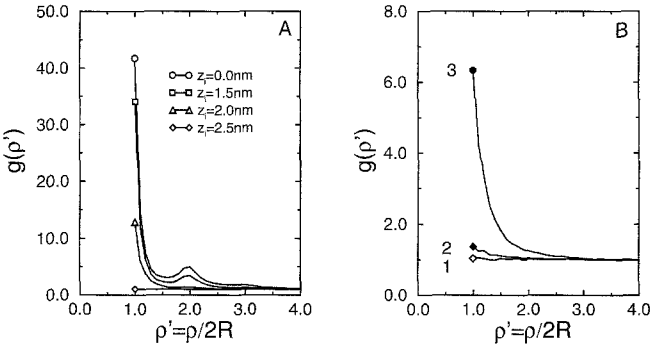

Fig. 3. Normalized radial distribution function $g(\rho')$ for an oppositely charged particle system with radius R of 0.5 nm and α=1 (single charges) **A** Dependency of the radial distribution on the position of the charges as given in the legend. The parameters were as follows: the ionic strengths of both adjacent solutions were I=100 mM; the particle density was σ = 0.02 nm^{-2} and the input diffusion coefficient was D^o = 10^{-8}cm^2/s. Graph B shows the obtained radial distribution for modified system parameters. In curve 2, the charges were located on the membrane's surface (z_i = 2.5 nm) and the ionic strengths were lowered to 1 mM. Curve 3 corresponds to charge locations in the middle plane of the membrane but increased dielectric constant of the membrane (ε_m=10) For comparison, the curve obtained for surface charges of graph A (z_i=2.5 nm, I=100 mM) is repeatedly shown (curve 1)

lateral correlations, obtained for charge positions in the middle plane of the membrane, were almost cancelled if a higher membrane dielectric constant of 10 was assumed (curve 3 of Fig. 3B). Since the dielectric constant of biological membranes close to the membrane - solution interface is higher than in the interior, curve 3 of Fig. 3B allows conclusions about the extent of interactions of charged phospholipids (see discussion).

As expected, the lateral ordering is less pronounced for the larger, 1.5 nm particles (Fig. 4) since, to a first approximation, the maximal electric interaction energy is inversely proportional to the particle radius. However, comparing Fig. 3 and Fig. 4, a characteristic feature is apparent. The aggre-

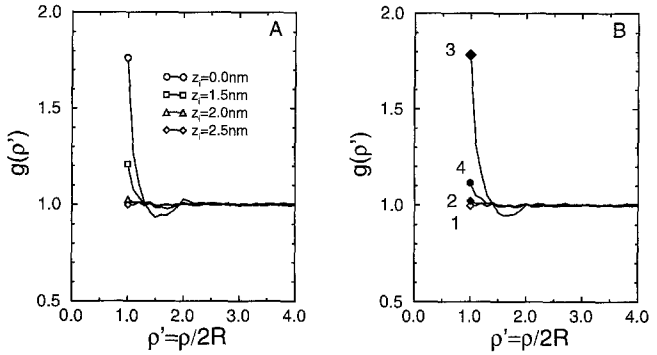

Fig. 4. Normalized radial distribution function $g(\rho')$ for an oppositely charged particle system with radius R of 1.5 nm. **A** Dependency of the radial distribution on the position of the charges as given in the legend. The following parameters were used: the charge number α was 1; the ionic strengths of both adjacent solutions were I=100 mM; the particle density was σ = 0.02 nm^{-2} and the input diffusion coefficient was $D^o = 10^{-9}$cm^2/s. Graph B shows the obtained radial distribution for modified system parameters. In curve 2, the single charges were located on the membrane's surface (z_i = 2.5 nm) and the ionic strengths were lowered to 1 mM. The charge number was set to 3 in curve 3 and the ionic strengths of both sides solutions were 1 mM. Curve 4 corresponds to charge locations in the middle plane of the membrane but increased dielectric constant of the membrane (ε_m = 10).For comparison, the curve obtained for surface charges of graph A (z_i = 2.5 nm, I=100 mM) is repeatedly shown (curve 1)

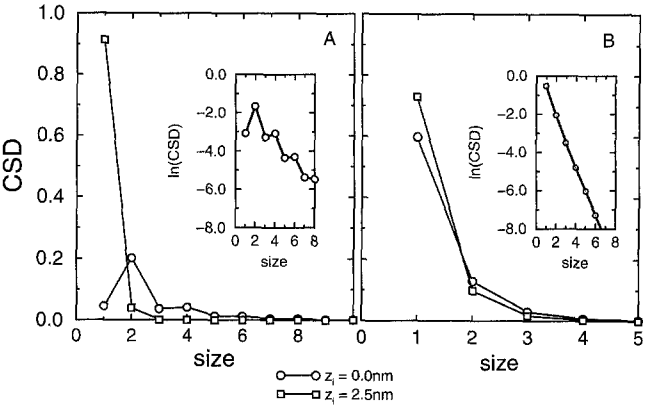

Fig. 5. Cluster size distribution function (CSD) of an oppositely charged particle system with single charges (α=1); i.e., the mean number of clusters of a certain size divided by the total number of particles. The particle radius R was taken as 0.5 nm in graph A and 1.5 nm in graph B, respectively. The two curves of each graph correspond to different charge locations as indicated in the legend. The parameters of the systems were: I=100 mM, σ = 0.02 nm^{-2} and $D^o = 10^{-9}(10^{-8})$cm^2/s for particles with radii 1.5 (0.5) nm. The insets show the logarithm taken from the CSD-function of systems with charge locations in the middle plane of the membrane

gation is very sensitive to the position of the charge with respect to the membrane - solution interface. For both particle radii, positioning charges only 1.0 nm beneath the membrane surface led to considerable lateral structuring as shown by the first peak in the radial distribution function. Remarkably, if single charges were placed directly onto the interface, no noticeable transient order was observed. Under these conditions the mean electric interaction energy per particle was approximately 2 to 3 orders of magnitude lower than the thermal energy as given by k_BT. This indicates that the Debye-screening of the charges is strongly dependent on the position of the charges. Only by assuming 3 elementary charges per particle and low ionic strengths of the adjacent solutions (I=1.0 mM) could a noticeable effect be observed for the larger particles (curve 3 in Fig. 4B).

The particle density also influenced the lateral distribution. Simulations with two different densities (σ = 0.02 nm^{-2} and σ = 0.04 nm^{-2}) revealed that increasing particle density was naturally accompanied by increased lateral order of equally charged particles and decreasing lateral order of oppositely charged particles (data not shown). This can be explained by an additional two-dimensional Debye-screening effect.

Unfortunately, the normalized radial distribution function $g(\rho')$ does not permit a direct comparison between the degree of clustering for different particle radii. For smaller particles $g(\rho' = 1)$ adopts greater values for the same degree of pair formation as for larger particles. It is therefore more informative to examine the cluster size distribution (CSD).

The CSD for the two selected particle systems distinguished by their radii are shown in Fig. 5. Conditions for low and pronounced, but reversible, aggregation were assumed. Surprisingly, a qualitatively different behaviour was observed for the two different systems. For the larger particles with radii of 1.5 nm and pronounced attractive particle-particle interactions in parallel, the CSD decayed almost exponentially with increasing cluster size whereas a clearly non-monotonous decay was obtained for the smaller particles (insets in Fig. 5). Furthermore, with smaller particles, cluster sizes with an even number of constituents were preferred. Apparently, the cluster energy as a function of the cluster size as well as of the cluster geometry must behave differently for the different radii. The mean electric energy per particle participating in the formation of isolated clusters of different sizes and geometries is plotted in Fig. 6. With growing cluster sizes, the electric energy decreases. The continued fall of the CSD is caused by entropic effects. Assuming as a first approximation a linear cluster size - cluster energy dependency, Fig. 6 reveals that triplets formed by small particles have relatively higher energy than quadruplets and are therefore relatively disfavoured. In contrast, triplets of the larger particles fall onto the straight line connecting the doublets and quadruplets. This is caused by the different slope of the electric potential decay in these distance ranges entailing different weighting of interactions between closest and more remote neighbours.

Nonequilibrium properties

While the equilibrium properties of the studied systems could also have been obtained by means of Monte Carlo simulation or analytical estimation, it is more complicated to characterize the non-equilibrium behaviour of the system, where the Brownian dynamics simulation is a simple, powerful method. As a local kinetic property we were interested in the lifetime of individual clusters. This characteristic time might be important for other cluster-mediated processes, e.g. transmembrane transport or chemical reactions and the like. The characteristic time of global lateral changes should depend on the interaction energy and on the mean interparticle distance as well as on the particle mobility. Finally, the dif-

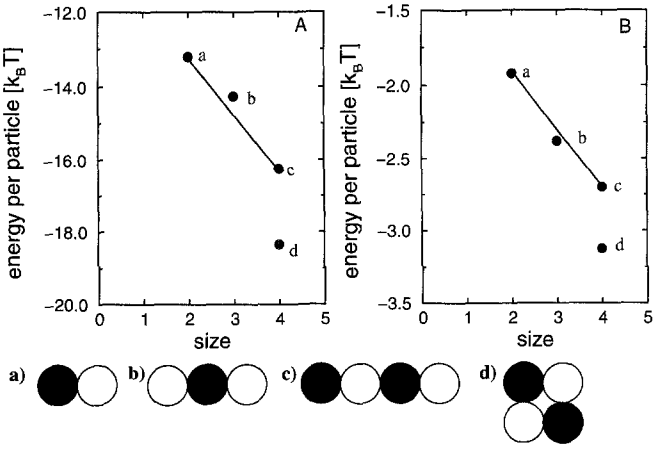

Fig. 6. Mean electric energies of particles participating in the formation of isolated clusters of different sizes, geometries and particle radii. Single charges were located in the middle plane of the membrane. The ionic strength I of both adjacent electrolyte solutions was 100 mM. The filled and empty circles correspond to positive and negative signs of the charges. The electric energy per particle of the clusters were calculated for different cluster types as depicted below the graphs

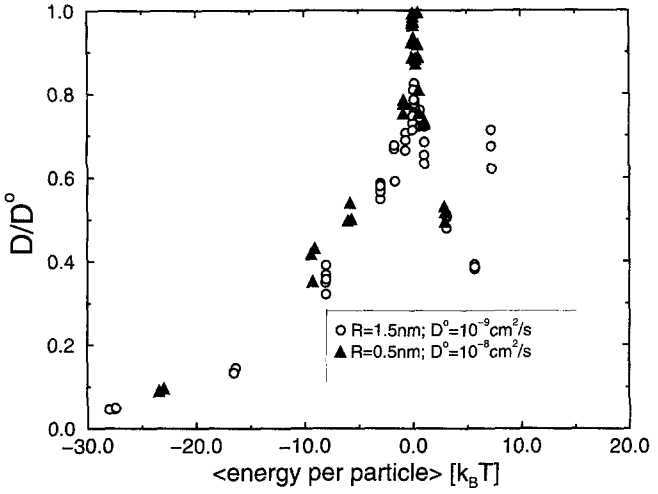

Fig. 7. Relative diffusion coefficient D/D^o as a function of mean electric interaction energy per particle in units of k_BT, where D is the simulated diffusion coefficient at equilibrium and D^o is the input diffusion coefficient (10^{-9}cm^2/s) The particle density and the radius were taken as σ = 0.02 nm^{-2} and R =1.5 nm, respectively. Positive interaction energies correspond to systems of equally charged particles only whereas the negative are obtained from particle systems with an equal number of positive and negative charges

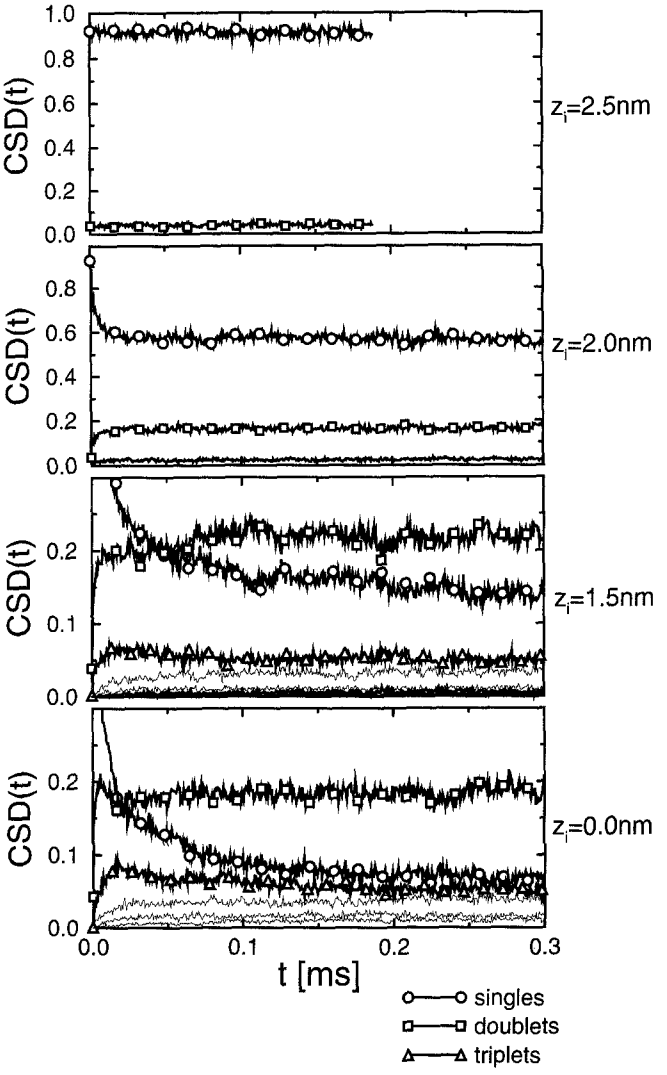

Fig. 8. Time evolution of the cluster size distribution function. The starting point t = 0 corresponds to a randomly distributed, non-overlapping particle system. The particle radius was 0.5 nm. The charges were positioned at various z coordinates as indicated in the graph. The ionic strength of both adjacent electrolyte solutions was 100mM and the charge number α was 1

fusion coefficient characterizes the kinetic properties of the particle system and describes the efficiency of the lateral transport within membranes.

Figure 7 summarizes the data for the obtained diffusion coefficients as a function of the mean electric energy per particle. Positive as well as negative energies characterize the lateral ordering of either a hexagonal lattice for equally charged particle systems or a quadratic array for oppositely charged systems. The diffusion coefficient decreased for both systems. Despite the different diffusion coefficients of the smaller and larger particles when the electric interaction was switched off, the dependency found for the relative diffusion coefficient on the mean interaction energy was similar. The relatively high energies required for a significant change of the diffusion coefficient as compared to the effect of crowding (see above) is remarkable. Figure 7 also reveals that the dependency of the diffusion coefficient on the mean electric interaction energy is not necessarily a monotonous function. Even though the mean energy increased by assuming other system parameters, the diffusion coefficient was observed to increase in parallel. It is clear that restrictions of particle motions are determined by the gradient of the interaction potential and not by its absolute value. There are situations where the selected system parameters allow diffusion of particles on a 'plateau' of high potential electric energy.

Figure 8 demonstrates how a condensed equilibrium particle arrangement starting from a random distribution of particles appears in time depicting the formation of larger clusters at the expense of smaller clusters. For smaller particles, equilibrium is nearly reached within about 0.2ms for strongly interacting particles (Lowest graph in Fig. 8). The slowest observed process was the decay of the number of single particles. Although increased particle radius is naturally accom-

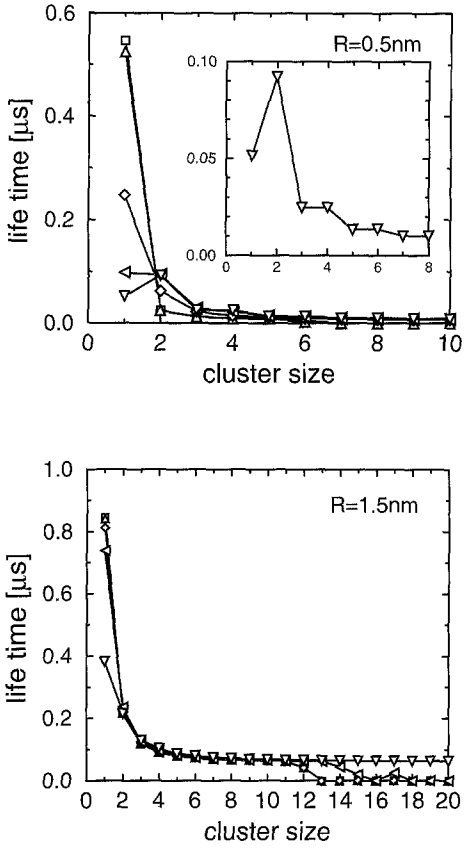

Fig. 9. Mean cluster life times for various particle systems. The life time was obtained by the mean observation time of a particular cluster measured with an discrete time interval of 1/10 of the time needed for a single particle to diffuse over a distance of 0.5 nm ($D = D^o$); i.e., the shell thickness that defines a neighbour in a cluster. The upper graph shows the observed life times for particles with a radius 0.5nm possessing a single charge. The curves correspond to: □ without electric interactions; △ z_i=2.5 nm; ◇ z_i=2.0 nm; ◁ z_i=1.5 nm and z_i=0.0 nm. The inset shows the magnified curve ▽. The lower graph shows the observed life times for particles with a radius 1.5 nm. The curves correspond to: △ z_i=2.5 nm; ◇ z_i=1.5 nm; ◁ z_i=0.0 nm and ▽ z_i=0.0 nm and charge to: △ z_i=2.5 nm; ◇ z_i=1.5 nm; ◁ z_i=0.0 nm and ▽ z_i=0.0 nm and charge number α=2 whereas the charge number α was unity in the preceding graphs. The ionic strength of both sides solutions was 100 mM

panied by a decreased diffusion coefficient, the equilibration times were almost identical for particle systems with a radius of 1.5nm. For systems of oppositely charged single charges located in the middle plane of the membrane, the population of singles reached its equilibrium frequency within about 0.3 ms and the population of doublets was stable within 0.15 ms (data not shown). This observed coincidence of the global change rates of the different particle systems is certainly explained by the different degree of occupancy of the membrane's area. In the case of smaller particles, a larger fraction of 'empty' area has to be traversed before the particles can aggregate which is partially compensated by the higher mobility and stronger lateral interactions at closer interparticle distances.

The fluctuations of the cluster size distribution in time, corresponding to the dynamic formation and dissociation of clusters, are depicted by mean observed cluster lifetimes in Fig. 9. For the smaller particles, a prolonged lifetime was observed for smaller to medium size clusters with increasing lateral interactions. The lifetimes were of the order of 0.05 ms. As already obtained for the CSD (Fig. 5), clusters with an even number of constituents are found to be favourable. They were preserved longer (Inset in the upper graph of Fig. 9). For particles with a radius of 1.5 nm, increased lateral interactions mainly resulted in the dynamic formation and dissociation of larger aggregates and not in the prolongation of the lifetimes of individual, small clusters. The mean lifetime of doublets remains almost constant (around 0.23 ms) for different strengths of lateral interaction. This is also a consequence of the different relative occupancies of the area. It should be noted, however, that the algorithm of lifetime determination (see section Materials and Methods) has systematic imprecisions caused by the all-or-none cutoff and the discrete time step of measurement.

Discussion

A variety of parameters control the lateral structure of biological membranes. Among these, networks formed by the membrane skeleton and chemical binding are certainly of major importance, although electric forces are always present and must be taken into account. Therefore we have attempted to delineate the influence of lateral electric interactions (representing a direct particle - particle potential) on the distribution of charged components in membranes via Brownian dynamics simulation of a simplified model system using parameters close to real biological situations.

The main conclusions are that the closest possible approach between oppositely charged sites of membrane particles and the position of the charge with respect to the interface are the principal components controlling the efficiency of electrostatic interactions. Significantly, placing the charge slightly beneath the membrane surface enormously enhanced the effect that electric interactions have on the lateral ordering (Figs. 3 and 4). This is due to the sensitivity of the electric potential distribution on the Debye-screening and to the low dielectric constant inside the membrane as compared to the electrolyte solution outside.

However, locating the charge underneath the membrane's surface increases the energy of the system by reducing the screening effect of the mobile ions in the solution and, in parallel, increasing the electric field energy inside the membrane because of the lower polarizability of the membrane material. Consequently, to bury a charge into a membrane interior requires additional energy. This burial energy is the difference in the Born (or self-) energies for two positions. A discussion of the role of electric forces in determining lateral order in membranes requires the simultaneous consideration of energetic aspects to estimate whether the differences in the Born energy for the simulated situations do not adopt unrealistically high values. The Born energy is given by Eq. (12),

$$E_{Born} = \int_0^{\alpha q} \varphi(Q) dQ. \qquad (12)$$

Here φ is the electric potential on the surface of the ion and q is the elementary charge. We approximated Eq. (12) by

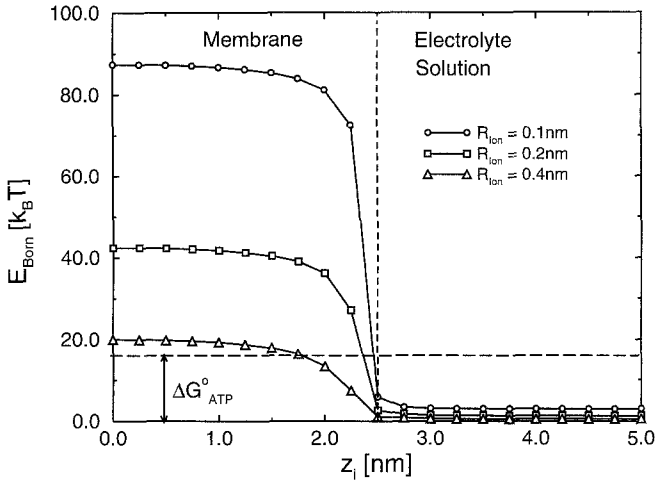

Fig. 10. Approximate Born energy (E_{Born}) as a function of the z-position of a charge with finite radius (R_{Ion}) as given in the graph. The Born energy was estimated by averaging the electric potential caused by single charges α=1) over the ion's surface. ΔG_{ATP} corresponds to the amount of energy available by hydrolysis of one molecule of ATP under standard conditions and pH=7.8 (Hoppe et al. 1977)

averaging the electric potential over the ions surface φ_m; i.e. $E_{Born} \approx \langle\varphi\rangle^2/(8\pi\varepsilon_0\varepsilon_{s/m})$. The results obtained as a function of ionic radius and location are plotted in Fig. 10. The Born energy decreases with increasing ion radius. As can be seen, transporting an ion deep into the membrane requires unreasonably high energies for small ions. (This is the main reason for the barrier function of a biological membrane). However, small depths may be achieved with energies comparable to biologically relevant values as demonstrated by comparison with the free energy available from hydrolysing one molecule of ATP (Hoppe et al. 1977). Consequently, charges well within the membrane are virtually possible only for large ions and at least locally increased polarizabilities. If the charges are of opposite signs they may release free energy *via* aggregation. Nonetheless, the energy barrier remains very high (some tens of k_BT) and charges deep within the membrane are still unfavourable. Honig and Hubell (1984) estimated a transfer energy for salt bridges formed by charge amino acids from water to the membrane interior of 17-27 k_BT. Thus, it is obvious that long-range direct charge-charge interactions play only a secondary role in the global arrangement of membrane components. This is supported by experimental results for membrane proteins in erythrocytes (Pearson et al. 1979). Lipid mediated aggregation and restrictions of the particle movement due to the cytoskeleton may be more dominant factors. We showed that for our charged model lipids (R=0.5 nm) no significant lateral structurization was found if the charges were located directly onto the membranes surface or the dielectric constant of the membrane was relatively high (Fig. 3). This is consistent with experimental results (Marassi and MacDonald 1991). In their study, no evidence for long-living associations between negatively and positively charged species of membrane lipids was found. Nonetheless, even in these cases, electric effects might well be important for the early steps of the inter-particle approach until other forces come in to play.

According to the data of Sitaraman et al. (1991), the mean charge number per membrane protein is +3.6 on the cytosolic and -2.95 on the periplasmic side of the membrane. Simulations performed with these charges assigning them simultaneously to one of the two opposing surface positions of the particles showed that the repulsive forces between the equally charged particles would have almost no consequences for their lateral distribution (data not shown). Only interactions between charges on the same side of the membrane were considered. Trans-effects were estimated to be far too small to result in considerable interactions.

Naturally, proteins are polyelectrolytes with several charged groups exposed to the aqueous solution and, contrary to our assumptions in the performed simulations, these charges are not necessarily placed on the rotation axis of the molecule. Eccentric charge positions would result in increased local pairwise electrostatic interaction compared to our simulations. Rotational degrees of freedom have to be introduced in future simulations and real membrane proteins should be studied in order to study these questions in more detail .

The thickness of the membrane was 5nm with a homogeneous low dielectric constant of ε_m = 3. For biological membranes the thickness of the hydrophobic core is reported with 2.5-3.0 nm and $\varepsilon_m \approx 2$ flanked by layers of polarizable phospholipid headgroups with 1.0-1.5 nm thickness each. For this polar region, dielectric constants of the order of 10-30 have been estimated (Honig et al. 1986). Considering those additional layers explicitly would not change the general results. This would merely require a deeper insertion of the charges into the membrane at the same expense of Born free energy. It is the relation between the pairwise electrostatic attractive interaction energy which increases with positioning the charges deeper into the membrane and the Born energy which increases simultaneously that is finally important. These considerations show that the charge positions used with respect to the interface are relative and model dependent while the qualitative results obtained still have general validity.

Discrete charges within membranes as a part of a larger protein molecule are surrounded by regions of higher polarizability. Calculations of the electric potential of discrete charges taking into account cylindric areas of higher dielectric constant have been reported (Sancho and Martinez 1991). Future studies, especially those devoted to local electrostatic effects, should certainly use more detailed approximations of the lateral electric potential distribution. Although it can be concluded from our simulations that long range electrostatic effects in membranes are limited, the importance of electrostatic interactions for other membrane processes such as variations in ion transport characteristics (Frausto et al. 1992) or field sensitive switching elements should not be underestimated.

Acknowledgement. This work was partially supported by a grant from the Deutsche Forschungsgemeinschaft (DFG) Do 410/1-1. The authors are grateful to David Thomas and Simon Hubbard for critically reading the manuscript. Helpful comments in preparation of the manuscript by André Juffer are gratefully acknowledged.

Appendix

Assuming a model consisting of an electrolyte solution, a membrane and an electrolyte solution and the corresponding parameters as shown in Fig. 1, the position of the fixed charge q is given by the two components of the cylindrical coordinate system ρ_i and z_i. Within the framework of Debye-Hückel approach, the following system of linearized Poisson-Boltzmann differential equations are obtained for charge locations within the membrane or directly on the membrane's surface; namely,

$$region\ 1 : \Delta\varphi_1(\vec{\mathbf{r}}) = \kappa_1^2\varphi_1, \tag{13}$$

$$region\ 2 : \Delta\varphi_2(\vec{\mathbf{r}}) = -q\frac{\delta(\vec{\mathbf{r}} - \vec{\mathbf{r}}_i)}{\varepsilon_0\varepsilon_m}, \tag{14}$$

and

$$region\ 3 : \Delta\varphi_3(\vec{\mathbf{r}}) = \kappa_3^2\varphi_3, \tag{15}$$

where Δ is the Laplace' operator, ε_o is the absolute permittivity of vacuum, δ is the Dirac's Delta-function and $\vec{\mathbf{r}}$ is the position vector with the components ρ and z.
The boundary conditions are:

$$\varphi_1 = \varphi_2|_{z=-\frac{d}{2}}, \tag{16}$$

$$\varepsilon_s\frac{\partial\varphi_1}{\partial z} = \varepsilon_m\frac{\partial\varphi_2}{\partial z}|_{z=-\frac{d}{2}}, \tag{17}$$

$$\varphi_2 = \varphi_3|_{z=+\frac{d}{2}}, \tag{18}$$

$$\varepsilon_m\frac{\partial\varphi_2}{\partial z} = \varepsilon_m\frac{\partial\varphi_3}{\partial z}|_{z=+\frac{d}{2}} \tag{19}$$

and

$$\varphi = 0|_{|\vec{\mathbf{r}}-\vec{\mathbf{r}}_i|=\pm\infty} \tag{20}$$

The system of equations (Eqs. (13-15)) was solved by expanding the solutions in terms of Fourier- Bessel integrals. The solution is represented by the sum of the Coulomb potential of the fixed charge (Eq. (21)) and the potential of the induced charge at the interface.

$$\begin{aligned} &i : \varphi(\vec{\mathbf{r}}) = \frac{q}{4\Pi\varepsilon_m\varepsilon_0|\vec{\mathbf{r}} - \vec{\mathbf{r}}_i|};\\ and\quad &ii : \varphi(\vec{\mathbf{r}}) = \frac{q}{4\Pi\varepsilon_s\varepsilon_0|\vec{\mathbf{r}} - \vec{\mathbf{r}}_i|}e^{-\kappa|\vec{\mathbf{r}}-\vec{\mathbf{r}}_i|} \end{aligned} \tag{21}$$

i): fixed charge located in region 2; ii) fixed charge located in region 1 or 3.

If the fixed charge is placed inside the membrane or precisely onto the membrane surface, the solutions for resulting electric potential in the three regions of the system is given by Eqs. (22) and (23); namely:

$$\varphi_{1/3}(z,\rho) = \frac{q}{4\Pi\varepsilon_0\varepsilon_s}\int_0^\infty A_{1/3}(k)J_0(k|\rho - \rho_i|)dk, \tag{22}$$

and

$$\varphi_2(z,\rho) = \frac{q}{4\Pi\varepsilon_0\varepsilon_m}\int_0^\infty((\exp(-k|z - z_i| + B(k) + C(k))J_0(k|\rho - \rho_i|)dk, \tag{23}$$

where J_o is a zero-order Bessel function.

The coefficients $A_1(k)$, $A_3(k)$, $B(k)$ and $C(k)$ were obtained from the boundary conditions (Eqs. (16-20)):

$$A_{1/3} = \frac{2kf_{3/1}\exp(\frac{d}{2}\sqrt{k^2+\kappa_{1/3}^2} - \frac{d}{2}k - /+ (kz_i - z\sqrt{k^2+\kappa_{1/3}^2}))}{a_{3/1}\sqrt{k^2+\kappa_{1/3}^2} - k\xi b_{3/1}} \tag{24}$$

$$B(k) = \frac{(\sqrt{k^2+\kappa_3^2} - k\xi)f_1\exp(k(z_i - d + z))}{a_1\sqrt{k^2+\kappa_3^2} - k\xi b_1} \tag{25}$$

and

$$C(k) = -\frac{(\sqrt{k^2+\kappa_1^2} - k\xi)\exp(-k(d + z + z_i))}{\sqrt{k^2+\kappa_1^2} + k\xi} \left(1 - \frac{(\sqrt{k^2+\kappa_3^2} - k\xi)f_1\exp(k(2z_i - d))}{a_1\sqrt{k^2+\kappa_3^2} - k\xi b_1}\right) \tag{26}$$

where

$$a_{1/3} = (\sqrt{k^2+\kappa_{1/3}^2} - k\xi)\exp(-2dk) + (\sqrt{k^2+\kappa_{1/3}^2} + k\xi), \tag{27}$$

$$b_{1/3} = (\sqrt{k^2+\kappa_{1/3}^2} - k\xi)\exp(-2dk) - (\sqrt{k^2+\kappa_{1/3}^2} + k\xi), \tag{28}$$

$$\xi = \frac{\varepsilon_m}{\varepsilon_s}, \tag{29}$$

and

$$f_{1/3} = (\sqrt{k^2+\kappa_{1/3}^2} - k\xi)\exp(-k(d + /- 2z_i)) - (\sqrt{k^2+\kappa_{1/3}^2} + k\xi). \tag{30}$$

For charge locations outside the membrane, in this work used only for the estimation of the Born energy (Fig. 10), and a discussion of the above solutions see Arakelian et al. (1993). A C-program solving the given equations is available upon e-mail request to walther@embl-heidelberg.de.

References

Abney JR, Owicki JC (1985) Theories of protein-lipid and protein-protein interactions in membranes. In: Watts A, DePont JJ (eds) Progress in Protein-Lipid Interactions. Elsevier Science Publishers B.V., Amsterdam, pp 1-60

Allen MP, Tildesley DJ (1987) Computer Simulation of Liquids, Clarendon Press, Oxford

Arakelian VB, Walther D, Donath E (1993) Electric potential distribution around discrete charges in a dielectric membrane - electrolyte solution system. Colloid Polym Sci 270: 268-276

Brown GC (1990) Electrostatic coupling between membrane proteins. FEBS Lett 260: 1-5

Brussel SJ, Koch DL, Hammer,DA (1995) Effect of Hydrodynamic Interactions on the Diffusion of Intergral Membrane Proteins: Tracer Diffusion in Organelle and Reconstituted Membranes. Biophys J 68: 1828-1835

Cevc G (1990) Membrane electrostatics. Biochem Biophys Acta 1031: 311-382

Clarke RJ (1993) A theoretical description of non-steady-state diffusion of hydrophobic ions across lipid vesicle membranes including effects of ion-ion interactions in the aqueous solution. Biophys Chem 46: 131-143

Clegg RM, Vaz WLC (1985) Translational diffusion of proteins and lipids in artificial lipid bilayer membranes. A comparison of experiment with theory. In: Watts A, dePont JJ (eds) Progress in Protein- Lipid Interactions. Elsevier Science Publishers B.V., Amsterdam, pp 173-229

Davis ME, Madura JD, Luty BA, McCommon A (1991) Electrostatics and diffusion of molecules in solution: simulations with the Houston Brownian dynamics program. Comp Phys Commun 62: 187-197

Edmonds DT (1988) The different screening of electric charges and dipoles near a dielectric interface. Eur Biophys J 16: 255-257

Egberts E, Marrink SJ, Berendsen HJC (1994) Molecular dynamics simulation of phospholipid membrane. Eur Biophys J 22: 423-436

Ermak DL (1975) A computer simulation of charged particles in solution.I.Technique and equilibrium properties. J Chem Phys 62: 4189-4196

Forsten KE, Kozack DA, Lauffenburger DA, Subramaniam S (1994) Numerical solution of the nonlinear Poisson-Boltzmann equation for a membrane -electrolyte system. J Phys Chem 98: 5580-5586

Frausto JN, Läuger P, Apell HJ (1992) Electrostatic coupling of ion pumps. Biophys J 61: 83-95

Gennis RB (1989) Biomembranes- Molecular Structure and Function, Springer, New York

Hendrickson WA (1992) Receptor Structure: Models of Transduction. Curr Biol 2: 57-59

Honig BH, Hubell WL (1984) Stability of "salt bridges" in membrane proteins. Proc Natl Acad Sci USA 81: 5412-5416

Honig BH, Hubell WL, Flewelling RF (1986) Electrostatic interactions in membranes and proteins. Annu Rev Biophys Biophys Chem 15: 163-193

Hoppe W, Lohmann W, Markl H, Ziegler (eds) (1977) Biophysik - Ein Lehrbuch. Springer, Berlin Heidelberg New York, p 437

Jensen P, Barabási AL, Larralde H, Havlin Sh, Stanley E (1994) Controlling nanostructures. Nature 368: 22

Karyakin AV (1989) Simulation of protein clusterization in biological membranes (in russian). Biol Membrany 6: 218-225

Kozack RE, d'Mello MJ, Subramaniam S (1995) Computer Modelling of Electrostatic Steering and Orientational Effects in Antibody-Antigen Associations. Biophys J 68: 807-814

Lax M (1966) Classical Noise IV. Langevin methods. Rev Mol Phys 38: 541-566

Lemmon MA, Engelman DM (1992) Helix-helix interactions inside lipid bilayers. Curr Opi Struct Biol 2: 511-518

Marassi FM, MacDonald PM (1991) Response of the Headgroup of Phospahditylglycerol to Membrane Surface Charge as Studied by Deuterium and Phosphorus-31 Nuclear Magnetic Resonance. Biochem 30: 10558 -10566

Marcelia S (1976) Lipid mediated protein interaction in membranes. Biochem Biophys Acta 367: 165-176

Martinez G, Sancho M (1993) Electrostatic Interactions in gramicidin channels - III. Dielectric Model. Eur Biophys J 22: 301-307

McLaughlin S (1989)The electrostatic properties of membranes. Annu Rev Biophys Biophys Chem 18: 113-136

Mouritsen OG, Bloom M (1993) Models of Lipid - Protein Interactions in Membranes. Annu Rev Biophys Bimol Struct 22: 145-171

Nelson AP, McQuarrie DA (1975) The Effect of Discrete Charges on the Electrical Properties of a Membrane. I. J Theor Biol 55: 13-27

Northrup SH, Boles JO, Reynolds JCL (1988) Brownian Dynamics of Cytochrome c and Cytochrome c Peroxidase Association. Science 241: 67-70

Pearson RP, Hui SW, Stewart TP (1979) Correlative Statistical Analysis and Computer Modelling of intramembraneous Particle Distributions in Human Erythrocyte Membranes. Biochim Biophys Acta 557: 265-282

Pink DA, Laidlaw DJ, Chisholm DM (1986) Protein lateral movement in lipid bilayers. Monte Carlo simulation studies of its dependence upon attractive protein -protein interaction. Biochem Biophys Acta: 863: 9-17

Sancho M, Martinez G (1991) Electrostatic modelling of dipole-ion interactions in gramicidinlike channels. Biophys J 60: 81-88

Saxton MJ (1994) Anomalous Diffusion Due to Obstacles: A Monte Carlo Study. Biophys J 66: 394-401

Schnitzer JA, Lambrakis KC (1991) Electrostatic Potential and Born Energy of Charged Molecules within Phospholipid bilayer: Calculation via 3-D Numerical Solution of the Full Poisson Equation. J Theor Biol 52: 203-222

Sitaraman V, Parajpe SA Gangal AD (1991) Charge anisotropy across biological membranes: evidence and implications. Biochem Biophys Acta 1098: 336-343

Sperotto MM, Mouritson OG (1991) Mean-field and Monte Carlo Simulation studies of the lateral distribution of proteins in membranes. Eur Biophys J 16: 369-374

Zhou HX (1993) Brownian dynamics study of the influence of electrostatic interactions and diffusion on protein-protein association kinetics. Biophys J 64: 1711-16

Zwanzig R (1969) Langevin theory of polymer dynamics in dilute solution. Adv Chem Phys 15: 325-331